International Journal of Pharmaceutics 410 (2011) 1–8

Contents lists available at ScienceDirect

International Journal of Pharmaceutics

journal homepage: www.elsevier.com/locate/ijpharm

Assessment of the critical factors affecting the porosity of roller compacted ribbons and the feasibility of using NIR chemical imaging to evaluate the porosity distribution

Hanpin Lim [a], Vivek S. Dave [b], Linda Kidder [c], E. Neil Lewis [c], Raafat Fahmy [d], Stephen W. Hoag [a,*]

[a] School of Pharmacy, University of Maryland Baltimore, 20N Pine St., Baltimore, MD 21201, United States
[b] Lubrizol Advanced Materials, 9911 Brecksville Road, Brecksville, OH 44141, United States
[c] Office of New Animal Drug Evaluation, Center for Veterinary Medicine, FDA, Rockville, MD 20855, United States
[d] Malvern Instruments Inc.,7221 Lee Deforest Drive, Suite 300, Columbia, MD 21046, United States

ARTICLE INFO

Article history:
Received 17 August 2010
Received in revised form 24 January 2011
Accepted 21 February 2011
Available online 1 March 2011

Keywords:
Roller compaction
NIR chemical imaging
Porosity
Density
Roller compacted ribbon
Feed screw speed, Roller pressure, Roller speed, Quality by design, NIR-CI

ABSTRACT

The purpose of this study was to assess the porosity variation of roller compacted ribbons made using different process parameters; in addition, the feasibility of using near-infrared chemical imaging (NIR-CI) to evaluate porosity variations was examined. Ribbons of neat microcrystalline cellulose were compacted using a range of roll pressures (RP), roll speeds (RS) and feed screw speeds (FSS). The ribbon porosity decreased as RP increased with the exception of ribbons produced by the combination of high RS and low FSS where increasing RP increases the porosity of the ribbons. Lower RS was found to produce ribbons with lower porosity and the porosity increases as the RS increased. Increased FSS will decrease ribbon porosity at higher RS while it slightly increase the ribbon porosity at lower RS. A simple linear regression model showed NIR-CI was able to predict the ribbon porosity with a correlation of 0.9258. NIR-CI is able to characterize differences in porosity as a function of position on the ribbon where regions with lower porosity show higher absorbance. Nevertheless, NIR-CI is able to show sinusoidal variation in intensities along the roller compacted ribbon among all settings studied.

1. Introduction

Roller compaction has gained popularity in recent years as a dry granulation method to improve material flow and compressibility without the use of heat or solvents. This is especially beneficial when working with active ingredients that are heat or moisture sensitive and therefore cannot be wet granulated (Ende et al., 2007; Feng et al., 2008; Ghorab et al., 2007). Unlike the wet granulation process, roller compaction is a continuous process where a powder blend is compacted and consolidated into a sheet of solid mass by passing it between two counter-rotating rollers under pressure. The resulting product is called the roller compacted ribbon, which is then milled into granules of desired particle size (Peck et al., 2008). The continuous process has many advantages, consistent production, time scalability and fewer pieces of equipment, and therefore has the potential to reduce manufacturing costs (Daugherity and Chu, 2007).

The fundamental mechanisms of roller compaction are complex, and like other manufacturing techniques, product quality and performance depend upon raw material properties, machine construction and process variables. Material properties such as the particle size and morphology of the raw materials have been shown to affect the compaction properties of the ribbons, granule particle size distribution, flowability, content uniformity and compaction properties of the tablets (Bacher et al., 2007, 2008). Studies have shown that the tap and bulk density of the resulting milled granulation was consistently higher when made with smooth rolls than with a linear knurl (serrated) roll surface (Daugherity and Chu, 2007; Sheskey and Hendren, 1999). The volume of the serrated roll surface can significantly affect the ribbon thickness, as serration draws powder into the roll surface; the greater the serration volume, the thicker the ribbon (Daugherity and Chu, 2007). Process variables such as feed screw speed (FSS), roll speed (RS), roll pressure (RP), roll gap and milling condition can also impact the porosity distribution on roller compacted ribbons and the properties of the resulted granules (Daugherity and Chu, 2007; Peck et al., 2008).

Maintaining constant process parameters throughout the entire roller compaction operation does not always guarantee a completely homogenous ribbon. For example, the motion of the last flight of the spiral feed screw has been shown to create periodical sinusoidal density variation across the ribbon width and along the ribbon length (in the direction of ribbon output motion) as it

* Corresponding author. Tel.: +1 410 706 6865; fax: +1 410 706 0346.
E-mail address: shoag@rx.umaryland.edu (S.W. Hoag).

0378-5173/$ – see front matter © 2011 Elsevier B.V. All rights reserved.
doi:10.1016/j.ijpharm.2011.02.028

Table 1
Roller compaction operating parameters for this study.

Batch #	Roller speed (RPM)	Feed screw speed (RPM)	Roller pressure (MPa)	Feed screw speed/roller speed (RPM/MPa)
1	4	20	4	5
2	4	20	6	5
3	4	28	4	7
4	4	28	6	7
5	6	24	5	4
6	8	20	4	2.5
7	8	20	6	2.5
8	8	28	4	3.5
9	8	28	6	3.5

delivered powder to the compaction region (Guigon and Simon, 2003). Also, heat may be generated in the compaction region from friction between the rolls and compacted powder, causing variation in properties of the compacts during long compaction runs (Ghorab et al., 2007). Therefore, it is important to identify and develop a better understanding of the critical factors that affect the roller compaction process, so that they can be accounted for in the formulation design and be monitored during the process; this understanding of the process is needed to reliably and consistently maintain desired quality and product performance across a range of environments as part of the Quality-by-Design (QbD) approach (FDA, 2006).

Based on published research, the quality of the roller compacted granules are influenced by the porosity (i.e., relative density or solid fraction) distribution of the roller compacted ribbons, because porosity influences the ribbon strength and consequently variation in porosity will lead to a variation in the size distribution and density of the granules produced for a given milling condition (Miguelez-Moran et al., 2008, 2009; Tye et al., 2005; Wu et al., 2006). As observed by Gamble et al. (2010) increased in ribbon porosity of plastically deforming materials results in broader particle size distribution and reduce granule flow properties due to a greater volume of fine particles. Conversely, ribbons with lower porosity were shown to produce tablets with lower tablet crushing strength due to the work hardening of the plastically deforming materials.

The first part of this paper focuses on the characterization of bulk porosity variation of roller compacted ribbons when process parameters such as the FSS, RS and RP are changed. The FSS controls the material feeding rate into the compaction region of the rolls. Continuous flow of material into the compaction region of the rolls is important as under feeding can lead to less compaction while over feeding can cause over compression, which may even cause a block in the pre-compression zone. RS controls the dwell time of the material under pressure in the compaction region. A certain dwell time is necessary to allow particle rearrangement and bonding. Hence, short dwell times, for a given pressure, can lead to lamination and capping (in tablets) while long dwell times can lead to over compression causing the ribbon to flatten out and laminate (Peck et al., 2008). In large part, the RP controls the compaction pressure applied to the material. Higher roller pressure on plastically deforming materials such as the hydroxypropyl methycellulose was found to produce larger granules and the corresponding tablets were found to have a lower crushing strength due to work hardening (Peck et al., 2008).

The Process Analytical Technology (PAT), which is a part of the USA FDA's QbD initiative, seeks to better understand ingredient–process relationships and to establish appropriate control strategies, which includes real-time release testing, has generated increase interest in using nondestructive techniques to monitor and control the roller compaction process. These include single point near infrared spectroscopy (NIRS) to look at content uniformity, moisture content, relative density, tensile strength and Young's modulus. A strong correlation has been found between the NIRS predicted values and measurements obtained using a suitable reference method (Gupta et al., 2004, 2005a,b,c). However, method development for NIRS can be quite extensive, requiring the creation of calibration samples outside of "normal" ranges, and the constant maintenance of the model as it is applied in practice. As with many existing analytical techniques, NIRS averages spectral information from the entire data collection area, producing a single result. As the variation in chemical and physical properties over an area may actually influence the quality of the resulting product, a bulk characterization method may not be able to adequately probe the sample. Thermal effusivity results from roller compacted ribbons have also been shown to correlate with the solid fraction, tensile strength and Young's modulus of roller compacted ribbons but the technique suffers from several drawbacks (Ghorab et al., 2007). It can only accurately measure ribbons made by smooth rolls, it is dependent on the ability of the material to transfer heat through and between the particles, and as with NIRS it derives a single value across the measurement sampling area, instead of providing spatially resolved data. Other method includes X-ray micro-computed tomography where the authors determined the density distribution in roller compacted ribbons; however, it is inappropriate to be used in the density distribution study when more than one chemical composition is included (Miguelez-Moran et al., 2008, 2009).

To overcome some of the inherit limitations associated with bulk measurements, the second part of this paper will investigate the feasibility of determining the spatial dependence of ribbon porosity using near infrared-chemical imaging (NIR-CI), as differences in porosity across and along the ribbon's width and length can lead to variations in compact properties which can affect product quality (Gamble et al., 2010; Ghorab et al., 2007; Guigon and Simon, 2003). NIR-CI can be used as a tool to determine and better understand CQAs as part of a QbD approach. NIR-CI is a rapid and nondestructive analytical method that allows the collection of many thousands of NIR spectra (chemical information) as a function of position in the sample. These spectra can be compiled into an image (spatial information). In other words, in a single dataset the individual spectra are associated with a microscopic or macroscopic (depending upon image resolution) point in the sample which would enable a spatial description of porosity distribution in heterogeneous roller compacted ribbons without running separate calibration samples. Subsequent analysis of NIR-CI data enables qualitative and quantitative insight in the chemical and physical characteristics of heterogeneous samples (Lewis et al., 2006). These insights are valuable when measuring porosity of roller compacted ribbons as the pycnometer method averages the density across the sample, but it does not give information about the density variation across the sample. Using the porosity value measured by the pycnometer method together with NIR-CI analysis, NIR-CI is capable of determining the spatial porosity distribution, i.e., sample heterogeneity across the whole sample. To date no studies have been reported in the literature that have used NIR-CI to study the heterogeneity of roller compacted ribbons; hence, if successful this

study will provide a novel tool for roller compaction users to better understand the roller compaction process. Information about the chemistry and physical organization of the samples provided by NIR-CI is valuable for formulation development, and promotes process understanding, especially for complex, spatially varying process such as the roller compaction.

In this study, we have attempted to extend the application of NIR-CI to examine and understand the roller compaction process by monitoring the porosity variation across the ribbon width and length for different process parameters. The ribbons were composed of a single ingredient, Avicel® PH 102 and no API was used in this study, as the goal was to isolate the spatial distribution of porosity as a function of processing parameters. The porosity changes in the roller compaction ribbon are reflected in absorbance changes in the NIR spectra. The denser (less porous) a sample is, the greater the absorbance will be, while a very porous sample will have proportionally less material interacting with the incident NIR illumination, and will have correspondingly lower absorbance; analogous results were found for tablets (Cantor et al., 2011; Tabasi et al., 2008; Tatavarti et al., 2005).

2. Materials and methods

2.1. Materials

The Avicel® PH 102 grade of microcrystalline cellulose (MCC) was obtained from FMC Corporation (Newark, DE).

2.2. Preparation

2.2.1. Preparation of ribbons

Ribbons of neat Avicel® PH 102 were prepared using an Alexanderwerk® WP120V roller compactor (Alexanderwerk Inc., Horsham, PA) fitted with two counter rotating diamond knurl surface rolls of 12 cm diameter and 4 cm wide and a single feed screw. In order to produce ribbons with largest possible inter- and intra-variation in density, combinations of the highest and lowest settings achievable that could still produce a continuous ribbon, i.e., a long compacted strip without breaks, were determined, and values spanning this broad range of settings were selected for the experimental design. To produce more consistent ribbons the roller gap is typically controlled via feedback circuits in the roller compactor; however, these feedback circuits would damp out the differences in porosity because to achieve a consistent gap the FSS is dynamically adjusted during operation. To avoid this damping out of the response the roller gap was not fixed in this study, i.e., the automatic roller gap adjustment controls were turned off.

To collect samples for the bulk and NIR-CI porosity measurements, the ribbons were compacted using a RS of 4, 6 or 8 RPM, FSS of 20, 24 or 28 RPM, and RP of 4, 5 or 6 MPa; these combinations were studied using a factorial design with two levels three factors and a center point as shown in Table 1. For the porosity measurements, a single strip of roller compacted ribbon, at least 76 cm in length (about two times of the circumference of the roll) was collected for each roller compaction setting. The strip was then cut with a disposable microtome blade into smaller ~3 cm sections and stored for further analysis. To allow the roller compactor to reach steady state, samples were only cut from strips produced after 1–2 min of continuous operation. Thirteen consecutive samples from each roller compaction settings which represent a single rotation of the rolls (circumference of rolls = 38 cm) were measured except for the center point roller setting of RS: FSS: RP of 6 RPM: 24 RPM: 5 MPa where twenty-six samples were measured which represent two rotations of the rolls; these samples were used to study the repeatability of two consecutive cycles during roller compaction.

2.2.2. Porosity measurements

The true density of bulk Avicel® PH 102 powder was determined using a fully automatic gas displacement pycnometer-AccuPyc® 1330 helium displacement pycnometer (Micromeritics Instrument Co., Norcross, GA). Weight of Avicel® PH 102 powder were predetermined prior to the analysis. The pycnometer determines the volume of the Avicel® PH 102 powder by measuring the volume of gas displaced by the powder. The true density is derived automatically by the quotient of the sample weight entered and volume measured. The number of purges and runs were 10, purge and run fill pressures were 19.5 psig and the equilibration rate was 0.005 psig/min.

The envelope density of the Avicel® PH 102 roller compacted ribbons were determined using the GeoPyc® 1360 pycnometer (Micromeritics Instrument Co., Norcross, GA). The GeoPyc® 1360 pycnometer measures the envelope volume and calculates the envelope density of the roller compacted ribbons. The internal diameter of the chamber used, consolidation force and conversion factor selected in this study was 38.1 mm, 90 N and 1.1476 cm^3/mm, respectively. Dry*Flo* is used as the dry-fluid medium as recommended by the manufacturer. Using the true density of the Avicel® PH 102 powder, the GeoPyc® 1360 pycnometer reports percentage porosity of roller compacted ribbons using following equation:

$$P\% = \left(\frac{1 - \rho_{\text{envelope}}}{\rho_{\text{true}}}\right) \times 100$$

where P is the ribbon porosity, ρ_{envelope} is the envelope density and ρ_{true} is the true density. The single point bulk pycnometer determined mean porosity are the average of thirteen consecutive samples from each roller compaction settings except for the center point roller setting of RS:FSS:RP of 6 RPM:24 RPM:5 MPa where the mean porosity are the average porosity of twenty-six consecutive samples. The standard deviations are calculated based on these thirteen or twenty-six consecutive samples.

2.2.3. NIR chemical imaging measurements

Offline NIR-CI measurements on the roller compacted ribbons were collected with a Malvern SyNIRgi™ chemical imaging system (Malvern Instruments, Westborough, MA) in diffuse reflectance mode. Data sets of each ribbon were collected from 1300 to 2400 nm with a spectral point spacing of 10 nm and 16 co-added images per wavelength. The sample field of view (FOV) was approximately 40 mm × 32 mm corresponding to a magnification of about 125 μm/pixel (an image is 320 × 256 pixels). Dark image cubes used to correct for stray light and detector dark current were recorded using a low-diffuse reflectance material (a mirror), and background image cubes used to determine sample absorbance were recorded using a high-diffuse reflectance target (a white ceramic plate).

2.2.4. NIR-CI data analysis

All NIR-CI data were analyzed using ISys® 5.0 chemical imaging software (Malvern Instruments, Westborough, MA). Reflectance (R) data was generated using the following equation:

$$R = \frac{S - D}{B - D}$$

where S is the reflectance of a sample image cube, D is the reflectance of a dark image cube and B is the reflectance of a background image cube. The resulting sample data were converted to absorbance (A) using the following equation:

$$A = \log_{10}\left(\frac{1}{R}\right)$$

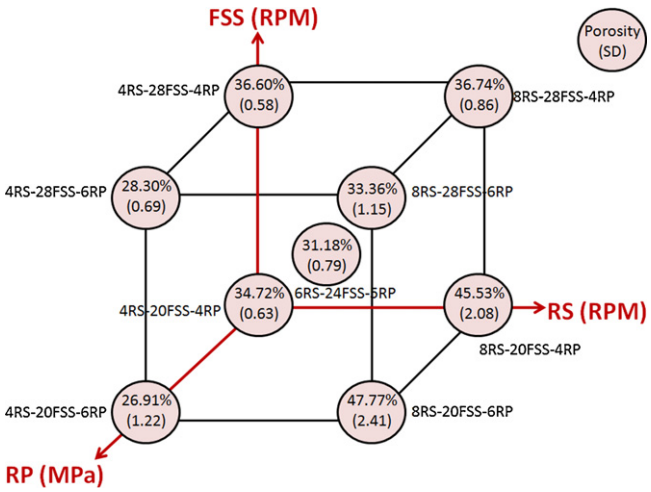

Fig. 1. Mean % porosity and corresponding standard deviation (SD) of Avicel® PH 102 prepared using different RS, FSS and RP ($n = 13$ for each setting except RS:FSS:RP of 6:14:5 where $n = 26$). Values determined using helium pycnometry.

Non-sample areas were masked to eliminate non-sample data and the image plane at 1310 nm of each sample was subtracted from each of the data cubes. This is equivalent to performing a single point baseline subtraction where there is no spectral contribution, the goal of which is to minimize scattering and other baseline effects, while preserving overall spectral intensity. The spectra from all image cubes were smoothed using a Savitsky–Golay smoothing filter (filter length 9, filter order 3). As there is a strong spectral feature for MCC at 2100 nm, and the roller compacted ribbons consist only of neat Avicel® PH 102, no spectral changes due to chemical variability are expected, the resulting linear shift in the baseline characterize by the mean intensity at this wavelength is proportional to the amount of Avicel PH 102 present. Hence, the mean intensity difference within and between samples is correlated to the porosity of the roller compacted ribbons using a simple linear regression. As described in Section 1, the denser (less porous) the Avicel ribbon is, the greater the spectral absorbance will be at 2100 nm.

The resulting color mapping with intensity scaling at 2100 nm from each roller compaction settings were compared to study the inter- and intra- porosity variation of roller compacted ribbons from different roller compaction settings. To confirm if the waffle pattern on the intensity map was due to density variation, the spectral were subjected to second derivative pre-processing as second derivatives is known to minimize baseline effects caused by physical variation in the sample. The waffle pattern will disappear if the waffle pattern shown in the intensity map is a result of density variation.

3. Results and discussion

3.1.1. Porosity of ribbons

Using the DOE described above and shown in Table 1 and the data analysis techniques described in Section 2.2.2, the single point bulk pycnometer determined mean porosity and standard deviation results for the ribbons are shown in Fig. 1. In Fig. 1 the three factors, RS, FSS and RP are each plotted as an axis and the two levels are indicated by the text adjacent to the porosity values in the circle, the center point also contains the experiment conditions in the adjacent text. The mean porosity of ribbons from different roller compaction settings ranged from 26% to 48%.

As shown in Fig. 1, the porosity decreased as RP increased from 4 MPa to 6 MPa at different RS and FSS settings as expected due to the higher RP exerted on the powder. An exception to this trend was seen for RS of 8 RPM and FSS of 20 RPM where increasing RP from 4 MPa (porosity = 45.53%) to 6 MPa (porosity = 47.77%) actually increased the ribbon porosity by 2.24%. These settings (8RS-20FSS-4RP and 8RS-20FSS-6RP) also produce ribbons with the highest porosity values for all the settings studied. At higher RS of 8 RPM, the rollers rotate faster, reducing compaction dwell time for material under pressure which in turn, reduces time for particle rearrangement and bonding. In addition, at the slower FSS of 20 RPM, the feed delivers less powder into the compaction region, which means there is a lower bulk density and higher porosity of the powder as it enters the compaction region, which enables more entrapped air to remain inside the powder in the compaction region during roller compaction. Combined with the higher RS, the entrapped air has a more difficulty leaving the powder mass as the dwell time is reduced; hence, the faster RS with shorter compaction dwell time and slower FSS with a slower powder delivery rate yields ribbons with the highest porosity among all settings studied.

Ribbons with the lowest porosity value were produced with RS of 4 RPM and RP of 6 MPa where the porosity value are 26.9% and 28.3% for FSS of 20 RPM and 28 RPM, respectively, due to the slower RS which in turn, allows a longer compaction dwell time for particle rearrangement and bonding under the higher RP. The effect of RS can also be seen when it is increased from 4 RPM to 8 RPM where the porosity of the ribbons are increased which is consistent with other researcher due to lower compaction dwell time (Gupta et al., 2005b). When FSS is increased from 20 RPM to 28 RPM at the high RS (8 RPM), the porosity of the ribbons decreased by 8.8% and 14.4% for RP of 4 MPa and 6 MPa, respectively. The authors believe this is due to less permeation of entrapped air occurs when powder is delivered to the compaction region at a higher rate when FSS is increased, hence, decreased the porosity of the ribbons. However, the FSS has minimal effect on the ribbons porosity at lower RS (4 RPM) where the ribbons porosity increased by 1.6% and 1.4% for RP of 4 MPa and 6 MPa when the FSS is increased from 20 RPM to 28 RPM. At the lower RS, the longer dwell time effect is predominant and the entrapped air becomes less affecting.

To summarize, ribbon porosity decreases as the RP increased with the exception of settings at high RS (8 RPM) with low FSS settings (20 RPM) where ribbon porosity was increased with increased RP. Higher RS was found to produce ribbons with higher porosity with the exception of high FSS (28 RPM) with low RP settings (4 MPa) where increasing RS does not significantly affecting the ribbon porosity. At higher RS (8 RPM), the ribbon porosity was reduced as the FSS is increased from 20 RPM to 28 RPM. On the other hand, the ribbon porosity was slightly increased as the FSS is increased from 20 RPM to 28 RPM at lower RS (4 RPM).

3.2. NIR chemical imaging

Fig. 2(a) is the color mapping of a roller compacted ribbon with intensity scaling at 2100 nm, which enables us to observe porosity variation across the roller compacted ribbons. The porosity variation within the Avicel® PH 102 ribbons are due to physical variation rather than chemical differences. Image contrast at 2100 nm disappeared (Fig. 2(b)) when subjecting to second derivative pre-processing, where this pre-processing method is known to minimize the impact of physical characterization while highlighting the chemical differences.

To determine the feasibility of NIR-CI to predict ribbon porosity, a calibration curve was created by plotting the measured single point bulk pycnometer porosity values of the roller compacted ribbons ($n = 100$) against the NIR-CI mean absorbance. The mean absorbance is calculated by averaging the absorbance intensity value of the bulk roller compacted ribbon at 2100 nm. The results are shown in Fig. 3(a), along with a simple linear regression fit

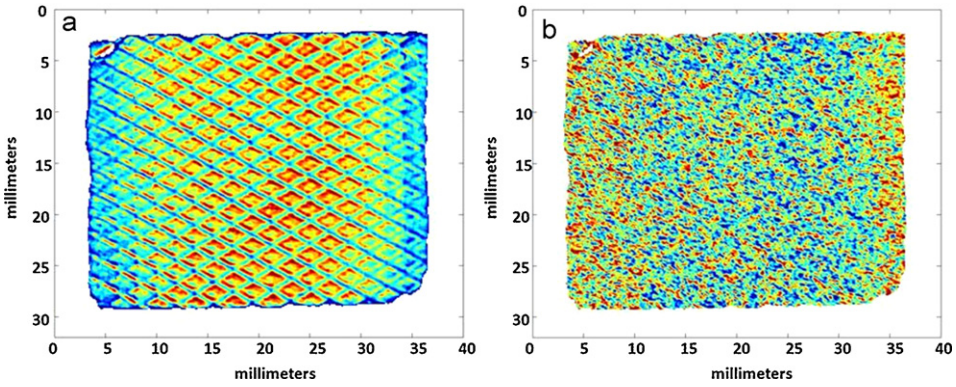

Fig. 2. (a) Color mapping of a neat Avicel® PH 102 ribbon. The colors of this image are based on absorbance at 2100 nm. (b) The image contrast disappeared when subjecting to second derivative pre-processing as it represents the porosity variation instead of chemical differences. (For interpretation of the references to color in this figure legend, the reader is referred to the web version of this article.)

yielding a calibration curve:

$$P = -280.27A + 136.99 \quad (R^2 = 0.9044)$$

where P is the porosity of the roller compacted ribbons and A is the mean absorbance at 2100 nm. The model was tested by predicting porosity results from NIR absorbance data on an independent set of ribbons ($n = 30$) whose values were not used in determining the calibration, see Fig. 3(b). The prediction yielded a strong correlation of 0.9258, suggesting that NIR-CI can be used to predict the porosity of the roller compacted ribbon even when the ribbon surface is not flat, as these ribbons were all made from diamond knurl surface rolls. The porosity and NIR absorbance are highly correlated where increasing NIR absorbance was observed with decreasing porosity (higher density) as there is more material interacting with the incident NIR illumination. This finding is consistence with the literature where density can affect absorbance and diffuse reflectance path length (Tabasi et al., 2008).

In addition to predicting the bulk porosity of roller compacted ribbons, NIR-CI inherently provides spatially resolved information, which can be used to show porosity variation on the order of the system magnification (~125 μm/pixel). As illustrated in Fig. 4, representative spectra from different spatial locations within a single ribbon show peak height variations. Because the ribbon is comprised of a single chemical species, the spectral differences become negligible when pre-processing steps that remove physical effects are applied, the data can be used to predict ribbon porosity and intra ribbon differences (see below), these spectral differences can confidently be attributed to physical (porosity) rather than other factors which could cause spectral differences. Fig. 4 shows an image whose contrast is based on the peak height (NIR absorbance) of the 2100 nm spectral band. Red areas have the lowest porosity (highest density), blue areas correspond to highest porosity (lowest density), and green areas are of intermediate porosity and density. Regions from within the diamond-shaped areas show the highest absorbance at 2100 nm (highest density or lowest porosity) due to the diamond knurl surface of the rollers where this spatial area is more tightly compacted than the depressed areas on the roller surface surrounding it. Spectra from these depressed roller surface areas surrounding the diamonds should show lower NIR absorbance (higher porosity), and this is reflected in Fig. 4. The edge of the ribbon is expected to have the highest porosity as the Teflon edge guards were not in place allowing material to leaks out from this region during the compaction process. Representative single pixel spectra corresponding to the three distinct spatial regions are shown in Fig. 4. The red spectra with the highest NIR absorbance at 2100 nm is from the raised diamond area on the roller surface, the spectrum from a surrounding depressed area of the roller surface is shown in green, and an edge spectrum is in blue. The NIR-CI absorbance scans showed spectral shift as the porosity changes are consistent with the literature where spectral shifts were also observed using single point NIRS as the crushing strengths of the tablets changes as a result of density differences (Cantor et al., 2011; Tabasi et al., 2008; Tatavarti et al., 2005). NIR-CI is therefore able to characterize differences in porosity as a function of position on the ribbon.

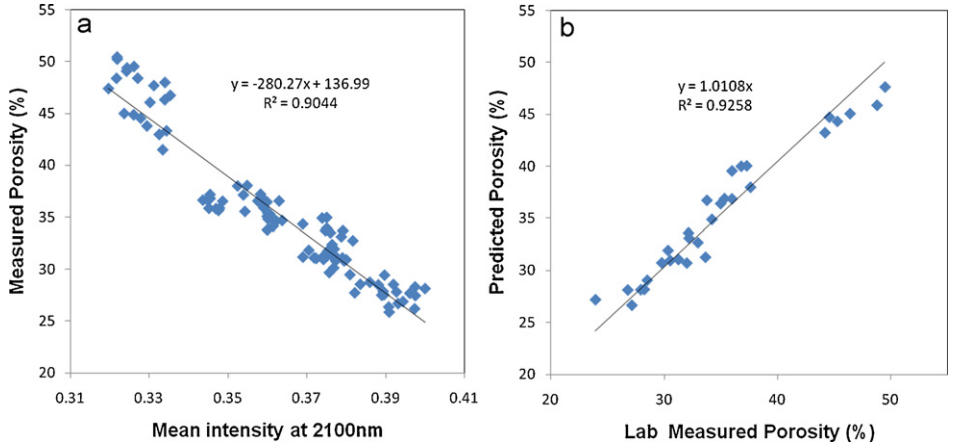

Fig. 3. (a) Simple linear regression model used to correlate the mean intensity at 2100 nm with the lab measured porosity. (b) Prediction model yielding R-squared value of 0.9258.

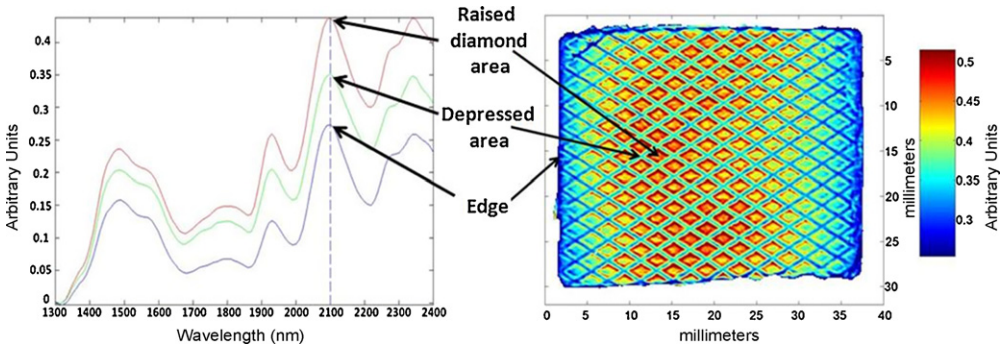

Fig. 4. The color mapping of the roller compacted ribbon at 2100 nm where red spectrum corresponding to the regions within the raised diamond area, green spectrum corresponding to the regions within the depressed area and blue spectrum corresponding to the regions around the edge. (For interpretation of the references to color in this figure legend, the reader is referred to the web version of this article.)

To assess the porosity variation across the roller compacted ribbon width, and also between the roller surface raised diamond areas and depressed areas, three samples with known bulk average porosity (26.35%, 36.56% and 50.27%) were compared. The line projection plot (see Fig. 5(a)) was used to show the ribbon's intensity with respect to the location where the blue line was drawn on the intensity images (see Fig. 5(b)). Both the line projection plot and intensity images show porosity variation across each ribbon's width, the center showing higher intensity than the edges as seen by the slight curvature of the line plots, suggesting lower porosity values at the central regions. More variations are found between the raised diamond area and depressed area, seen as the high frequency changes in the plots. The first sample shown in Fig. 5(b) showed highest intensity (mean absorbance = 0.3947) corresponding to the lowest measured bulk porosity (26.35%), whereas the third sample with the lowest intensity (mean absorbance = 0.3285) corresponding to the highest measured bulk porosity (50.27%). The porosity variation between the raised diamond and depressed regions is due to the diamond knurl surface rolls where it allows more material to deposit per volume on the depressed area than the raised diamond area. As a result, the diamond regions showed lower porosity (or higher density) comparing to the depressed area. The edges of the ribbons showed highest porosity due to powder leakage.

To assess the axial porosity variation of the roller compacted ribbons, individual sample produced by each roller compaction setting were concatenated (digitally stitched together) to examine the porosity variation across the width and along the length of an entire roller compacted ribbon and between different roller compaction settings, the individual 3 cm images of the ribbon were concatenated to produce a single image of the entire ribbon. The intensity map shown in Fig. 6 shows sinusoidal variation in intensities along the roller compacted ribbon among all settings studied, indicative of a corresponding sinusoidal variation in the porosity. This finding is consistent with other researchers (Guigon and Simon, 2003; Simon and Guigon, 2003) where sinusoidal density variation was found in a compacted sodium chloride ribbon, determined by measuring the distribution of light transmitted through the ribbon. The periodicity of variation is due to the periodicity of the FSS and the motion of the last flight of the spiral feed screw as it rotates to deliver powder to the compaction region. The powder located at the last flight of feed screw will get densified and the powder does not move much if it has higher porosity than the powder located in the space between the rolls, whereas if the powder at the last

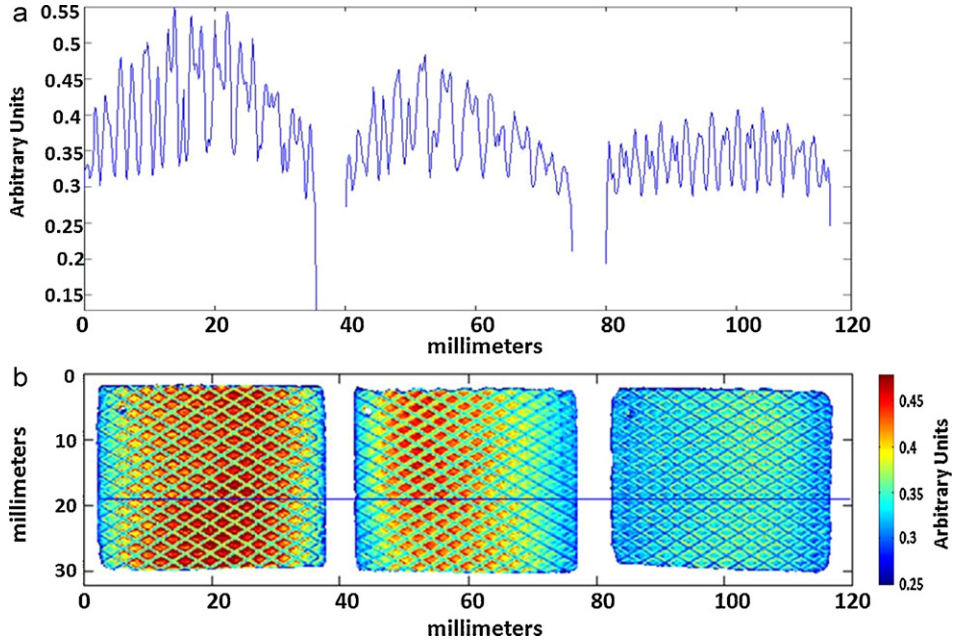

Fig. 5. (a) Line projection plot shows porosity variation across the sample width, and between the raised diamonds and depressed area. (b) Intensity images of three samples with known measured porosity at 2100 nm. The measured bulk porosity for the sample on the left, center and right are 26.35%, 36.56% and 50.27%, respectively, and the mean absorbance are 0.3947, 0.3674 and 0.3285, respectively.

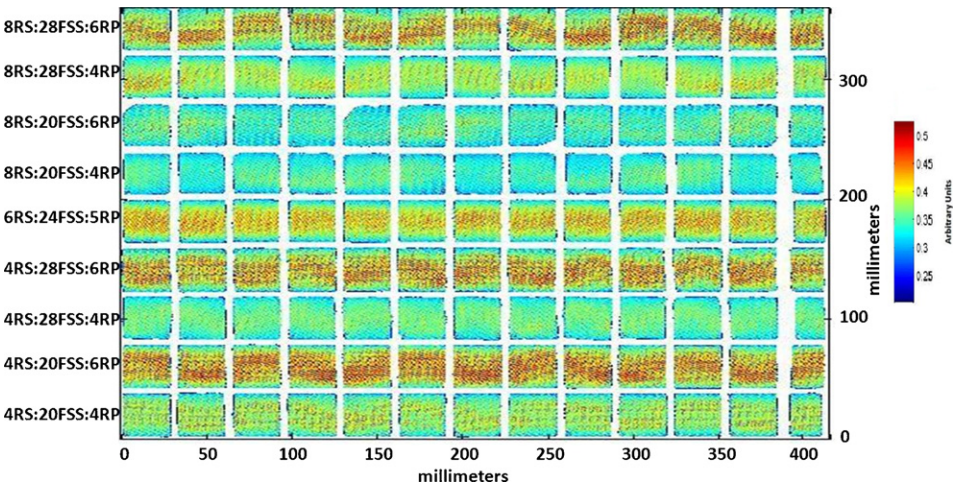

Fig. 6. Intensity map of roller compacted ribbon prepared by various RS, FSS and RP.

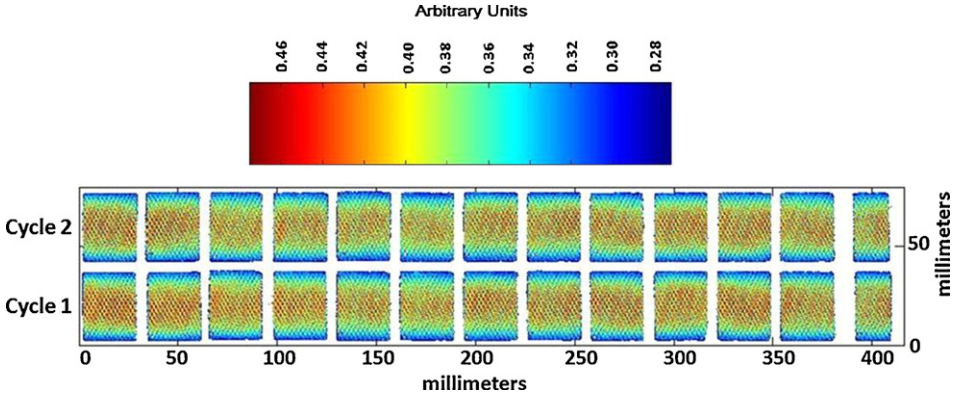

Fig. 7. Intensity map of roller compacted ribbon prepared by two continuous roller compaction cycle with RS, FSS and RP settings of 6 RPM, 24 RPM and 5 MPa, respectively.

flight of screw has equal porosity as the powder located in the space between the rolls, it will move (Guigon and Simon, 2003; Simon and Guigon, 2003). Thus, the non-continuous pulsing densification process from the feed screw results in sinusoidal porosity variation along the roller-compacted ribbons. In fact, the NIR-CI shows increased sinusoidal periodicity as the FSS is increased and the same FSS show same periodicity. In addition, NIR-CI allowed us to study the repeatability and variation across and along the ribbons width and length made by two consecutive cycles of roller compaction as seen in Fig. 7 where the periodicity porosity variation were identical for the two continuous cycle showing the process is repeatable.

4. Conclusions

In this study, the effects of various roller compaction settings (RS, FSS and RP) on the ribbon porosity were investigated. The study show that ribbon porosity increases as the RS increased due to the reduction of compaction dwell time for particles undergo rearrangement and bonding. FSS has negative effect in changing the ribbon porosity at higher RS where increased FSS will decrease ribbon porosity while it has minor positive effect at lower RS. At lower RS, the compaction dwell time and RP predominant. It was also observed that increased RP will decrease ribbon porosity, because higher pressures are exerted on the powder by the rollers. In addition, the study demonstrated the use of NIR-CI as a nondestructive tool to determine the ribbon porosity. The technique can also be used to investigate the porosity distribution across the width and along the length of the ribbons.

Acknowledgements

The authors gratefully acknowledge Nick Hayes of Volkmann, Inc. and Malvern Instrument, Inc., and the FDA for their support and advice.

References

Bacher, C., Olsen, P.M., Bertelsen, P., Kristensen, J., Sonnergaard, J.M., 2007. Improving the compaction properties of roller compacted calcium carbonate. Int. J. Pharm. 342, 115–123.

Bacher, C., Olsen, P.M., Bertelsen, P., Sonnergaard, J.M., 2008. Granule fraction inhomogeneity of calcium carbonate/sorbitol in roller compacted granules. Int. J. Pharm. 349, 19–23.

Cantor, S., Hoag, S.W., Augsburger, L.L., D. Ellison, C., Khan, M.A., Lyon, R.C., 2011. NIR spectroscopy applications in the development of a compacted multiparticulate system for modified release. Pharm. Sci. Technol., doi:10.1208/s12249-010-9580-z.

Daugherity, P.D., Chu, J.H., 2007. Investigation of serrated roll surface differences on ribbon thickness during roller compaction. Pharm. Dev. Technol. 12, 603–608.

Ende, M.T.A., Moses, S.K., Carella, A.J., Gadkari, R.A., Graul, T.W., Otano, A.L., Timpano, R.J., 2007. Improving the content uniformity of a low-dose tablet formulation through roller compaction optimization. Pharm. Dev. Technol. 12, 391–404.

FDA, 2006. ICH Harmonised Tripartite Guideline: Quality Risk Management Q9., http://www.fda.gov/downloads/Drugs/GuidanceComplianceRegulatoryInformation/Guidances/ucm073511.pdf.

Feng, T., Wang, F., Pinal, R., Wassgren, C., Carvajal, M.T., 2008. Investigation of the variability of NIR in-line monitoring of roller compaction process by using Fast Fourier transform (FFT) analysis. AAPS Pharm. Sci. Technol. 9, 419–424.

Gamble, J.F., Tobyn, M., Dennis, A.B., Shah, T., 2010. Roller compaction: application of an in-gap ribbon porosity calculation for the optimization of downstream granule flow and compactability characteristics. Pharm. Dev. Technol. 15, 223–229.

Ghorab, M.K., Chatlapalli, R., Hasan, S., Nagi, A., 2007. Application of thermal effusivity as a process analytical technology tool for monitoring and control of the roller compaction process. AAPS Pharm. Sci. Technol. 8, 7.

Guigon, P., Simon, O., 2003. Roll press design - influence of force feed systems on compaction. Powder Technology. 130, 41–48.

Gupta, A., Peck, G.E., Miller, R.W., Morris, K.R., 2004. Nondestructive measurements of the compact strength and the particle-size distribution after milling of roller compacted powders by near-infrared spectroscopy. J. Pharm. Sci. 93, 1047–1053.

Gupta, A., Peck, G.E., Miller, R.W., Morris, K.R., 2005a. Effect of the variation in the ambient moisture on the compaction behavior of powder undergoing roller-compaction and on the characteristics of tablets produced from the post-milled granules. J. Pharm. Sci. 94, 2314–2326.

Gupta, A., Peck, G.E., Miller, R.W., Morris, K.R., 2005b. Influence of ambient moisture on the compaction behavior of microcrystalline cellulose powder undergoing uni-axial compression and roller-compaction: a comparative study using near-infrared spectroscopy. J. Pharm. Sci. 94, 2301–2313.

Gupta, A., Peck, G.E., Miller, R.W., Morris, K.R., 2005c. Real-time near-infrared monitoring of content uniformity, moisture content, compact density, tensile strength, and Young's modulus of roller compacted powder blends. J. Pharm. Sci. 94, 1589–1597.

Lewis, E.N., Kidder, L.H., Lee, E., 2006. NIR chemical imaging as process analytical tool. Innovations Pharm. Technol., 107–111.

Miguelez-Moran, A.M., Wu, C.Y., Dong, H.S., Seville, J.P.K., 2009. Characterisation of density distributions in roller-compacted ribbons using micro-indentation and X-ray micro-computed tomography. Eur. J. Pharm. Biopharm. 72, 173–182.

Miguelez-Moran, A.M., Wu, C.Y., Seville, J.P.K., 2008. The effect of lubrication on density distributions of roller compacted ribbons. Int. J. Pharm. 362, 52–59.

Peck, G.E., Soh, J.L.P., Morris, K., 2008. Dry granulation. In: Augsburger, L.L., Hoag, S.W. (Eds.), Pharmaceutical Dosage Forms: Tablets. Informa Healthcare USA, Inc., New York, pp. 303–336.

Sheskey, P.J., Hendren, J., 1999. The effects of roll compaction equipment variables, granulation technique, and HPMC polymer level on a controlled-release matrix model drug formulation. Pharm. Technol. 23, 90–106.

Simon, O., Guigon, P., 2003. Correlation between powder-packing properties and roll press compact heterogeneity. Powder Technology. 130, 257–264.

Tabasi, S.H., Fahmy, R., Bensley, D., O'Brien, C., Hoag, S.W., 2008. Quality by design. Part I. Application of NIR spectroscopy to monitor tablet manufacturing process. J. Pharm. Sci. 97, 4040–4051.

Tatavarti, A.S., Fahmy, R., Wu, H., Hussain, A.S., Marnane, W., Bensley, D., Hollenbeck, G., Hoag, S.W., 2005. Assessment of NIR spectroscopy for nondestructive analysis of physical and chemical attributes of sulfamethazine bolus dosage forms. AAPS Pharm. Sci. Technol. 06, E91–E99.

Tye, C.K., Sun, C.C., Amidon, G.E., 2005. Evaluation of the effects of tableting speed on the relationships between compaction pressure, tablet tensile strength, and tablet solid fraction. J. Pharm. Sci. 94, 465–472.

Wu, C.Y., Best, S.M., Bentham, A.C., Hancock, B.C., Bonfield, W., 2006. Predicting the tensile strength of compacted multi-component mixtures of pharmaceutical powders. Pharm. Res. 23, 1898–1905.